Supporting Information

Assembly of Platinum Nanoparticles and Single-atom Bismuth for Selective Oxidation of Glycerol

Ning Huang,‡[a] Zihao Zhang,‡[b] Yubing Lu,[c] Jinshu Tian,[d] Dong Jiang,[b] Chenguang Yue,[a] Pingbo Zhang,[a] Pingping Jiang,[a] and Yan Leng.[a]*

Characterizations

The Fourier Transform Infrared (FT-IR) spectrum was obtained on Nicolet 360 FT-IR instrument. The nitrogen adsorption isotherms and pore size distribution curves were measured using a BELSORP-MINI analyzer at liquid nitrogen temperature (77 K). XRD patterns were collected on the Bruker D8 Advance powder diffractometer using Ni-filtered Cu/Kα radiation at 40 kV and 20 mA, from 5 to 90º with a scan rate of 5º/min. The CHN elemental of catalysts was carried out on an elemental analyzer Elementar virio macro cube. The content of Pt and Bi in the sample was determined on 1100 inductively coupled plasma emission spectrometer (ICP-AES). X-ray photoelectron spectroscopy (XPS) was performed with a PHI 5000 Versa Probe X-ray photoelectron spectrometer equipped with Al Ka radiation source. The basicity of the catalyst was determined by CO_2-TPD desorption with Micromeritics BelCata II equipment. The atomic geometry configuration was detected by in-situ CO-DRIFTS using Tensor 27 spectrometer. The sample was pretreated with H_2/He atmosphere (1/9, V/V, 50 mL/min, 5 ºC/min) at 150 ºC for 1.5 h. After purging with He (50mL/min) for 1 h and colling to 30 ºC, the spectrum is collected every five minutes until the signal peak remains unchanged. The catalyst morphology and element distribution were analyzed by FEI Themis Z spherical aberration corrected transmission electron microscope (STEM) and energy dispersive X-ray spectroscopy (EDS, voltage 20 kV).

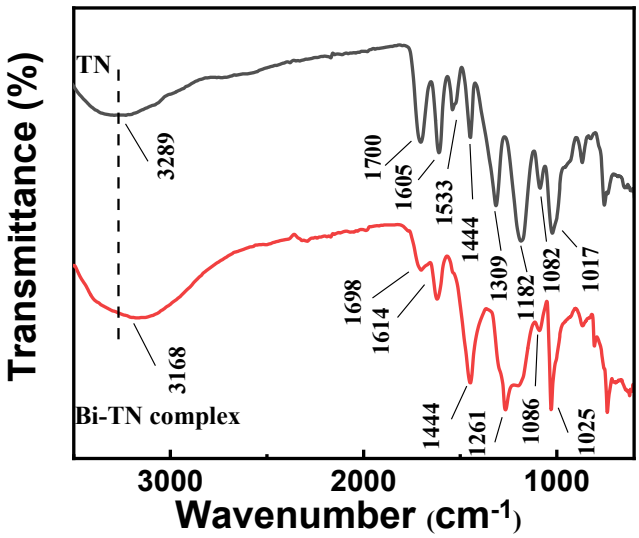

Figure S1. FT-IR spectra of TN and Bi-TN complex.

The FT-IR spectrum of tannin displayed typical vibration peaks for -Ar-OH bending (1309 cm^{-1}), -C-O- stretching (1182 cm^{-1}, 1017 cm^{-1}), and aromatic C=C stretching (1605 cm^{-1}). Notably, in the case of Bi-TN, the vibrations at 1309 cm^{-1}, 1182 cm^{-1}, and 1017 cm^{-1} shifted to wave-numbers of 1261 cm^{-1}, 1197 cm^{-1}, 1025 cm^{-1}, respectively, and the intensity of the band for aromatic C=C was remarkably decreased as compared with that of tannin. Moreover, the peak at 3289 cm^{-1} for -Ar-OH stretching of TN shifted to 3168 cm^{-1}. These observations indicate the possible coordination between Bi^{2+} and -Ar-OH that cause the formation of -Ar-O_2-Bi-O_2-Ar- networks.

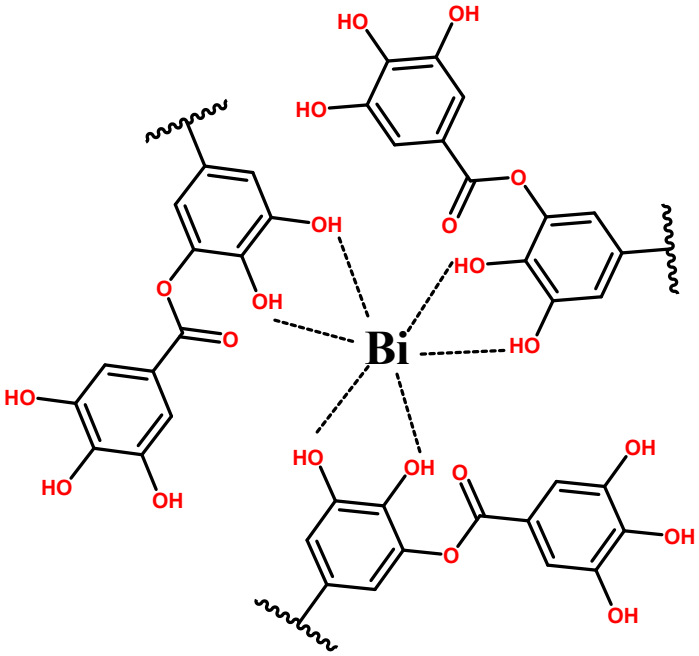

Figure S2. Proposed structure of Bi-TN.

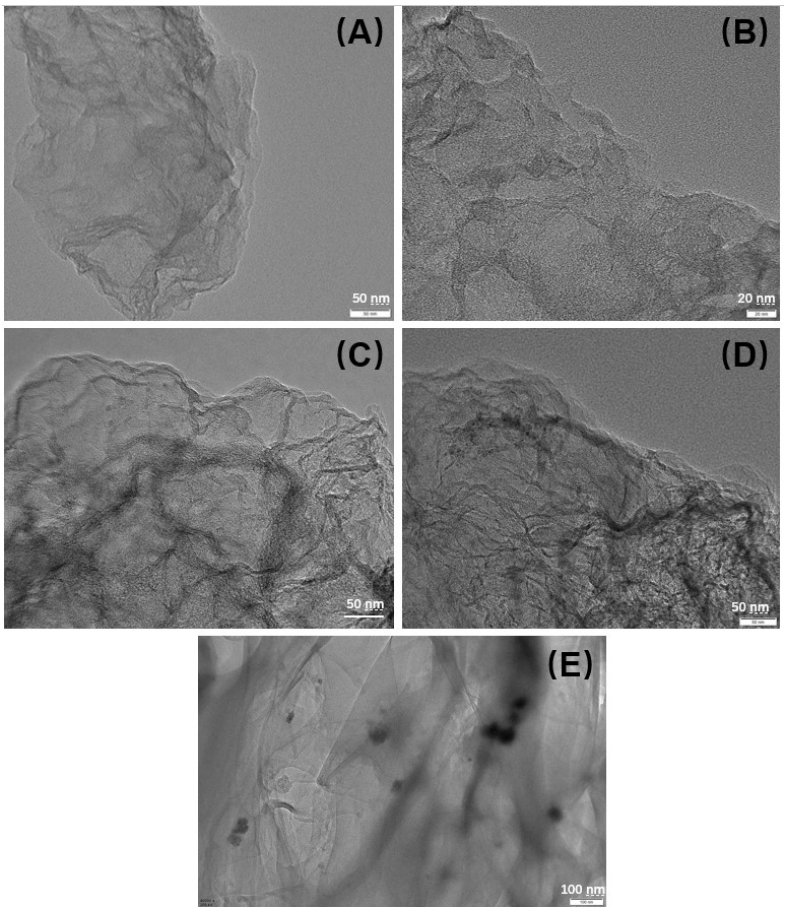

Figure S3. TEM images of (A) 0.05Bi@NC, (B) 0.1Bi@NC, (C) 0.15Bi@NC, (D) 0.2Bi@NC, and (E) 0.1Bi@C.

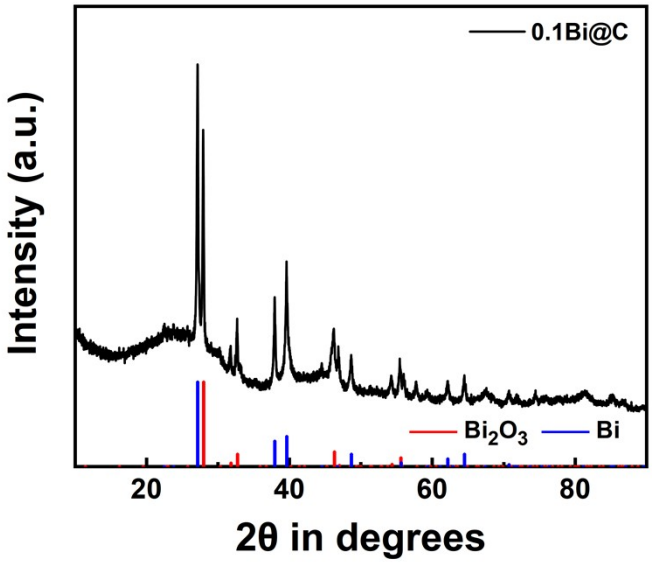

Figure S4. XRD pattern of 0.1Bi@C.

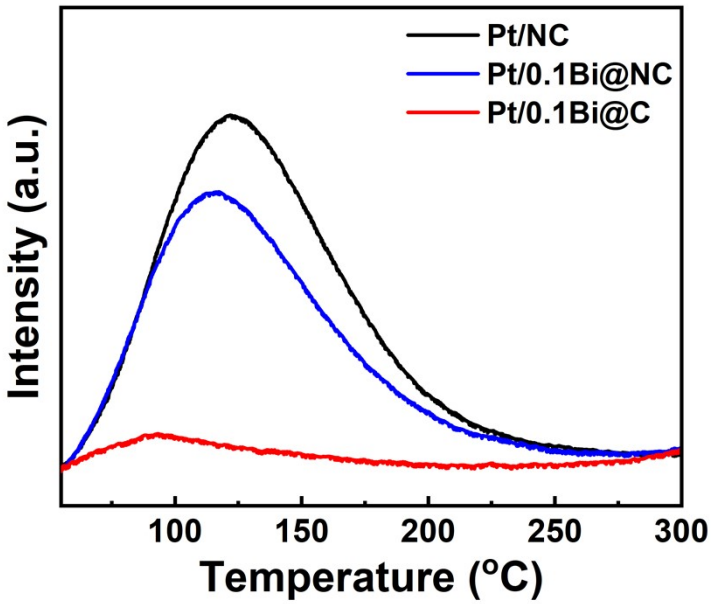

Figure S5. CO_2-TPD spectra of Pt/NC, Pt/0.1Bi@C, and Pt/0.1Bi@NC.

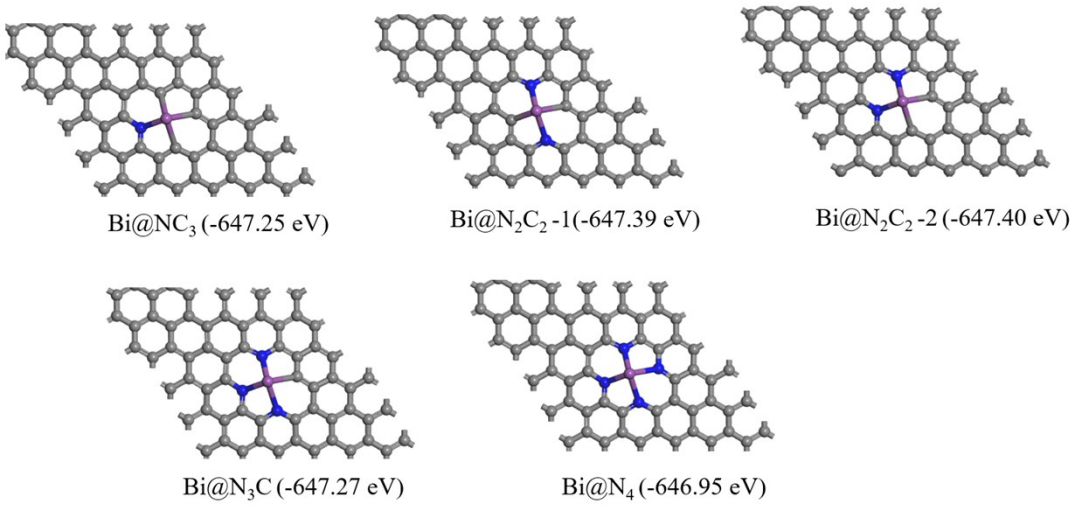

Figure S6. Different structures of Bi@NC with electronic energy.

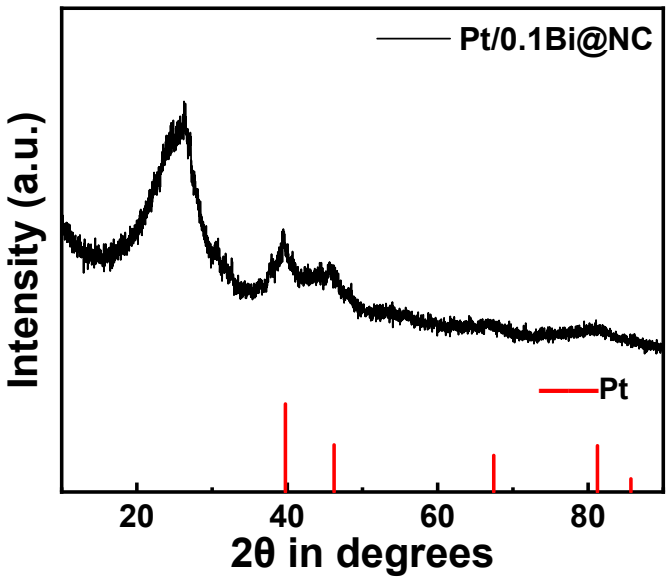

Figure S7. XRD pattern of Pt/0.1Bi@NC.

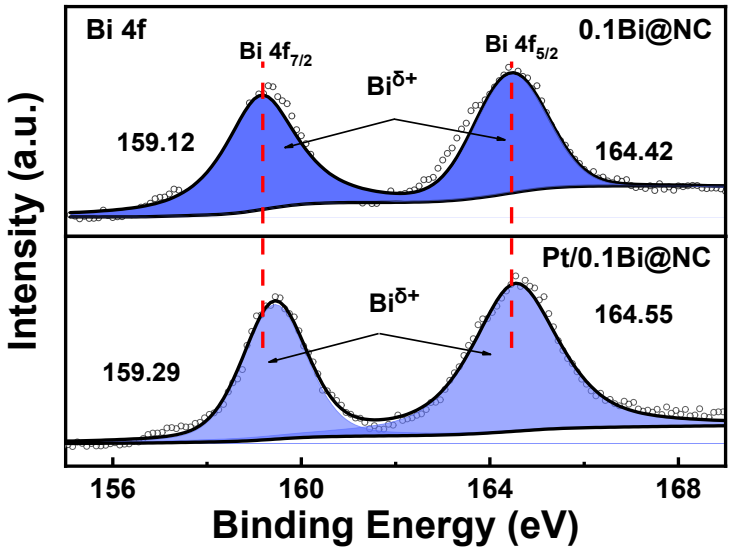

Figure S8. Bi 4f XPS spectra of 0.1Bi@NC and Pt/0.1Bi@NC.

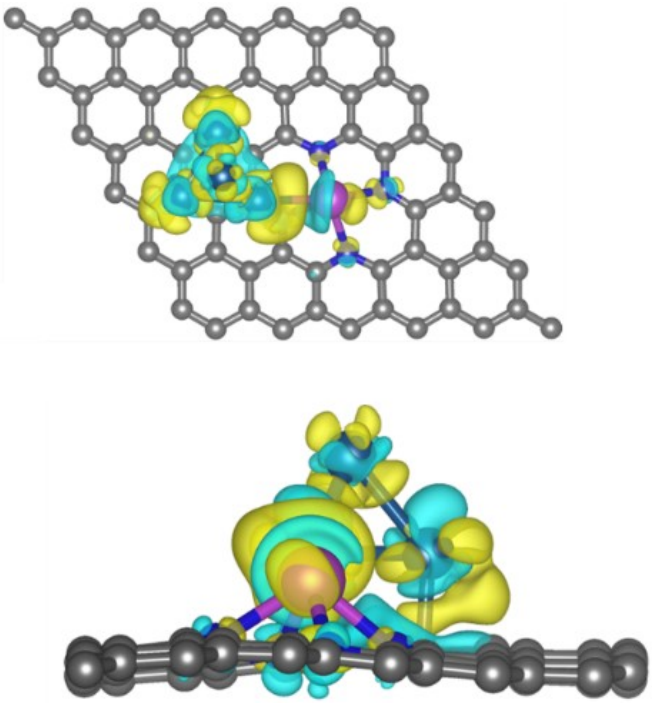

Figure S9. Charge density difference of isosurfaces of Pt/0.1Bi@NC. The cyan/yellow colors indicate the regions of electron loss/gain. Isosurfaces of charge density are set to 0.003 e·Bohr^{-3}.

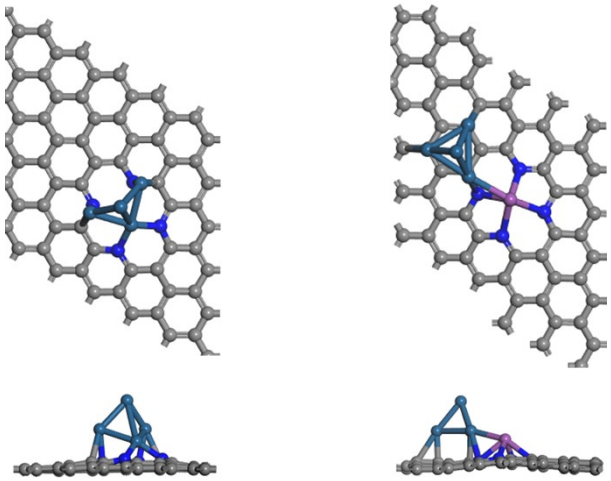

Figure S10. The optimized slab models of Pt/NC and Pt/0.1Bi@NC.

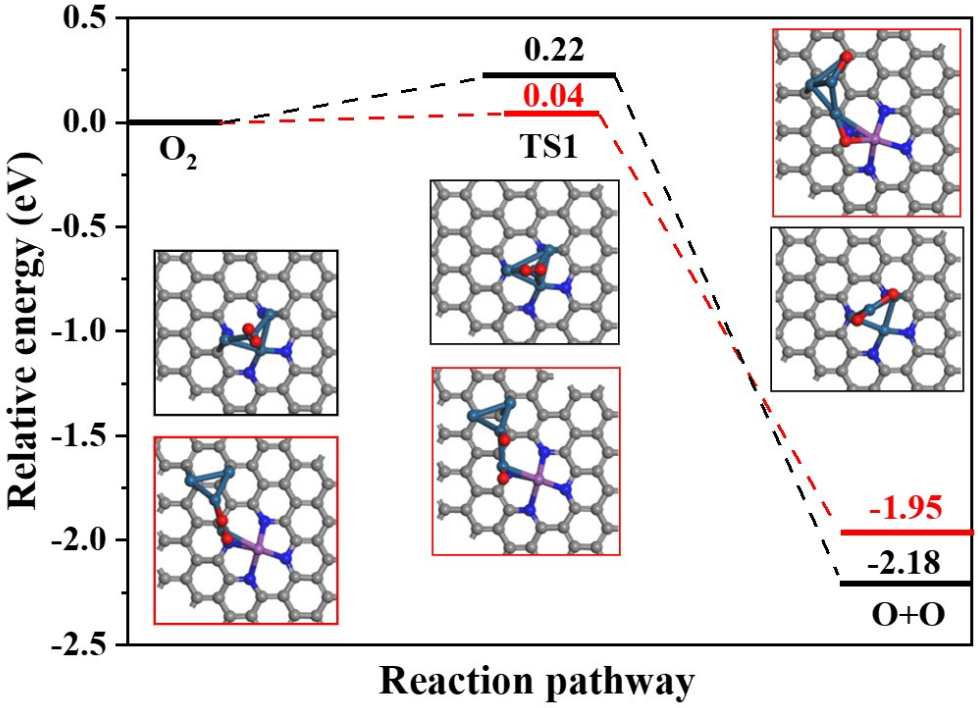

Figure S11. Energy profiles for O_2 dissociation on Pt/NC and Pt/0.1Bi@NC with the initial structure, transition state and the final structure.

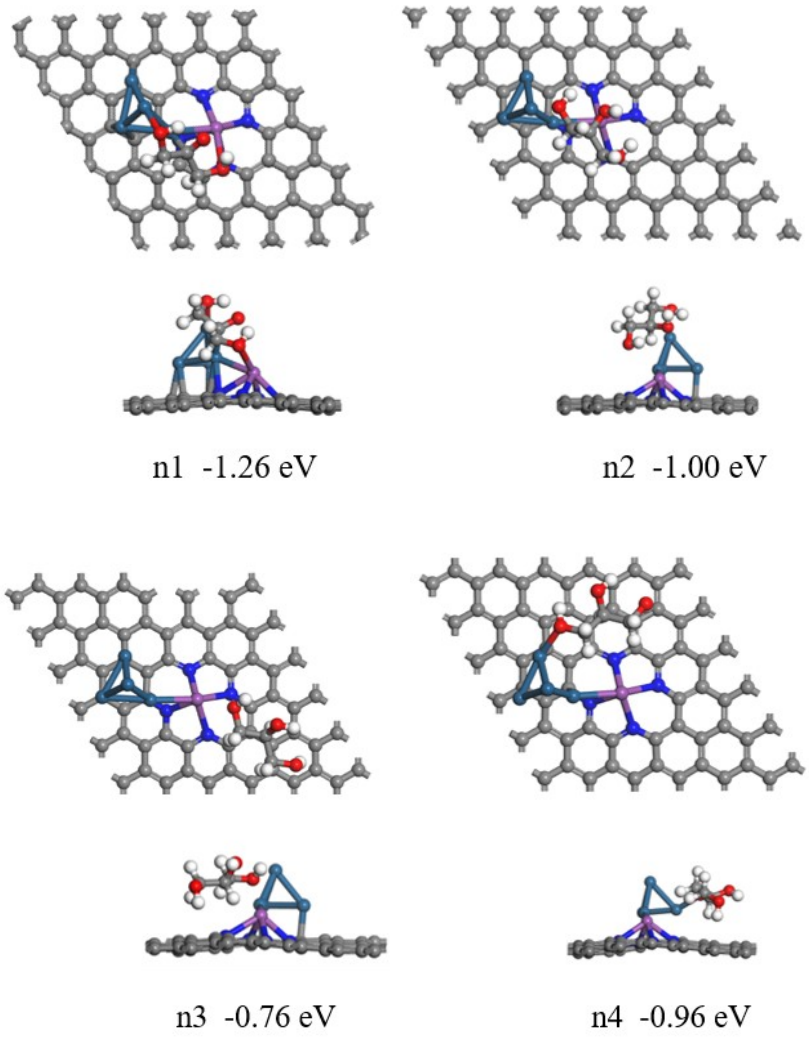

Figure S12. The different adsorption configurations of $C_3H_8O_3$ on Pt/0.1Bi@NC.

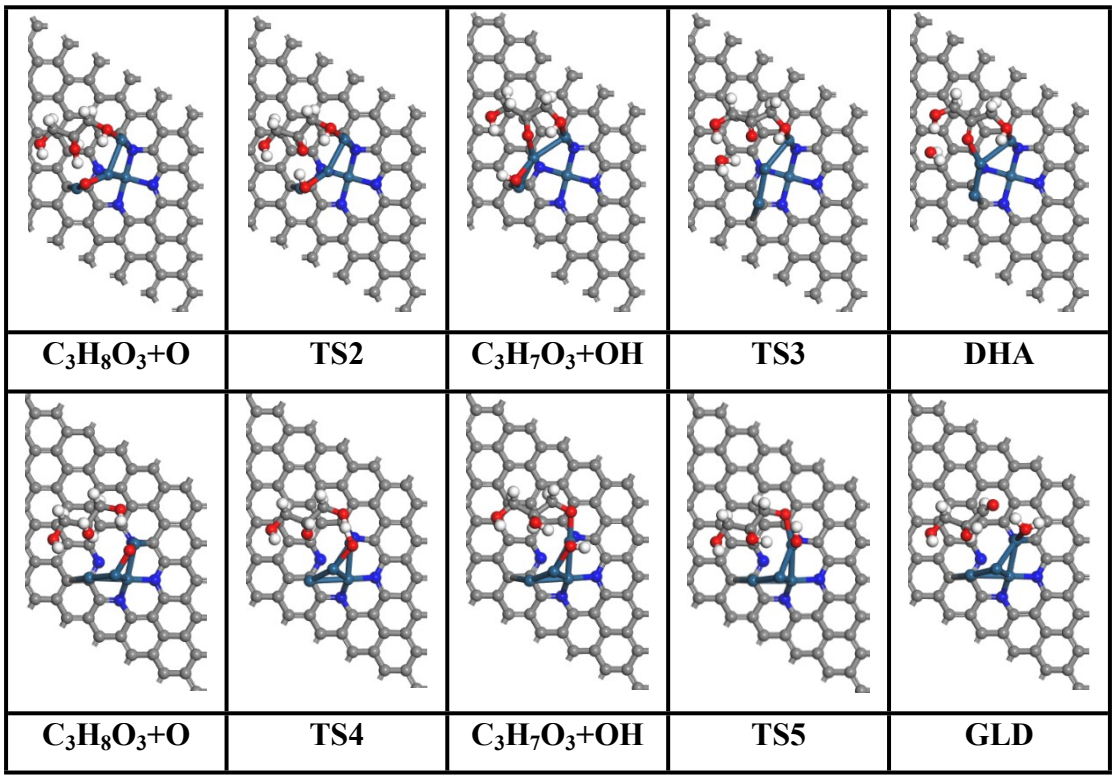

Figure S13. Glycerol selective oxidation to DHA on Pt/NC with the initial structure, transition state and the final structure.

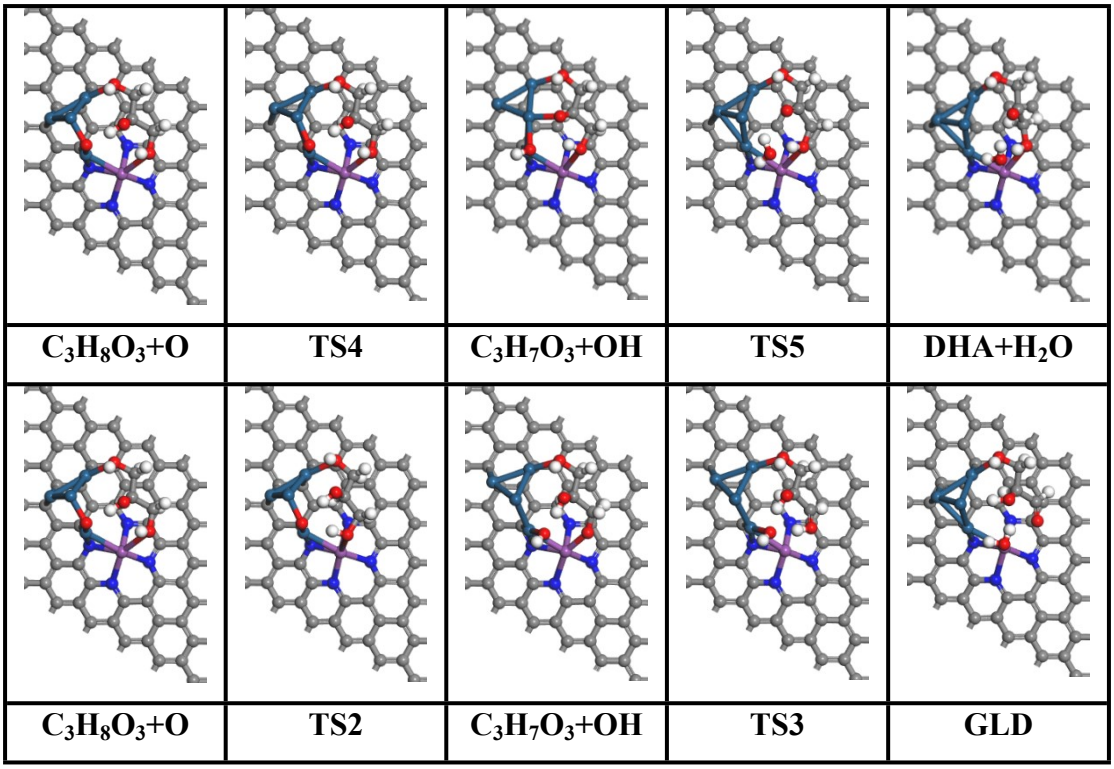

Figure S14. Glycerol selective oxidation to DHA on Pt/0.1Bi@NC with the initial structure, transition state and the final structure.

Table S1. The actual Pt and Bi contents of different bimetallic Pt-Bi catalysts obtained from ICP-AES

Samples	Bi (wt%)	Pt (wt%)	Bi/Pt ratio
Pt/0.05Bi@C	0.53	1.42	0.37
Pt/0.08Bi@C	1.39	1.46	0.95
Pt/0.1Bi@C	2.57	1.58	1.63
Pt/0.15Bi@C	3.42	1.50	2.28
Pt/0.2Bi@C	4.56	1.48	3.08

Table S2. Results of catalytic oxidation of glycerol to DHA over various reported Pt-Bi-based catalysts.

Catalyst	Reaction condition	Con (%)	Sel (%)	Ref.
Pd–Bi/C	catalyst 0.05 g, aqueous solution of glycerol 20 g (5 wt.%), 80 °C, O_2 0.3 MPa, 4 h.	2	54	S1
$Pt_{5.0}Bi_{5.36}$/ AC7	glycerol/Pt = 1755 (mol/mol).120 °C, pH=4, O_2 300 mL/min, 7 h.	20	51	S2
5%Pt-5%Bi/C	catalyst 0.5 g, aqueous solution of glycerol 50 mL (0.1 g/mL), 60°C, O_2 150 mL/min, 6 h.	92	49	S3
$PtBi_5$/NCNT	catalyst 0.1 g, aqueous solution of glycerol 50 g (10 wt.%), 60°C, O_2 150 Ncm^3/min, 6 h.	30	56	
$PtBi_5$/NCNT (co-reduction)	catalyst 0.1 g, aqueous solution of glycerol 50 g (10 wt.%), 60°C, O_2 150 Ncm^3/min, 6 h.	25	47	S4
Pt/NCNT+ Bi/NCNT	catalyst 0.1 g, aqueous solution of glycerol 50 g (10 wt.%), 60°C, O_2 150 Ncm^3/min, 6 h.	34	53	
3Pt-xBi/SBA-15	catalyst 0.05 g, aqueous solution of glycerol 2.5 mL (200 mM), 30°C, 1 atm air, 15 h.	41	65	S5
Pt/N-MWCNTs-673	catalyst 0.1 g, aqueous solution of glycerol 10 mL (0.1 g/mL), 60 °C, O_2 0.5 MPa, 3 h.	40	14	S6
Pt-Bi/MWCNTs	catalyst 0.5 g, aqueous solution of glycerol 50 mL (0.1 g/mL), 60 °C, O_2 150 cm^3/min.	50	51	S7
3%Pt–0.6%Bi/C	catalyst 0.35 g, aqueous solution of glycerol 175ml (1M), 70°C, O_2 0.3 MPa, 4h.	80	60	S8
Pt/0.1Bi@NC	**catalyst 0.05 g, 5mL of 0.1M glycerol aqueous solution, 30°C, 1 atm air, 15 h.**	**86.8**	**87**	**Our work**

Table S3. Results of catalytic oxidation of glycerol over Pt/xBi@NC.

Catalyst	Bi/Pt ratio	Con (%)	C3 Sel (%)		
			DHA	GLA	HPVA
Pt/0.05Bi@NC	0.37	78.3	83.4	9.2	0.40
Pt/0.08Bi@NC	0.95	85.2	87.2	1.6	0.21
Pt/0.1Bi@NC	1.63	86.8	87.0	2.2	0.32
Pt/0.15Bi@NC	2.28	87.8	79.5	2.2	0.23
Pt/0.2Bi@NC	3.08	96.4	68.2	0.60	0.21

Reaction conditions: 50 mg of Pt/xBi@NC, 5 mL of 0.1 M glycerol aqueous solution, 303 K, 1 atm air, 15 h.

Table S4. Results of catalytic oxidation of glycerol over Pt/0.1Bi@NC with different reaction time and temperature.

Temperature (℃)	Time (h)	Con (%)	Sel $_{(DHA)}$ (%)	Sel $_{(GLA)}$ (%)
30	5	44.1	93.0	5.4
30	10	60.1	90.1	4.2
30	15	86.8	87.0	2.2
30	20	95.7	53.4	1.3
40	0.5	16.4	95.2	2.1
40	1	25.6	93.8	2.4
40	2	34.9	82.2	1.1
40	4	49.8	79.9	0.8
40	6	56.7	67.2	0.3
50	0.5	20.5	97.5	1.4
50	1	43.4	93.8	1.3
50	2	65.7	84.9	0.9
50	4	94.5	56.5	0.6
50	6	99.2	43.2	0.5
60	0.5	40.6	92.7	1.2
60	1	53.2	82.3	1.1
60	2	81.1	69.8	0.7
60	4	95.2	53.4	0.1
60	6	99.2	38.8	0.1

REFERENCES

S1. S. Hirasawa, H. Watanabe, T. Kizuka, Y. Nakagawa and K. Tomishige, *Journal of catalysis* 2013, ***300***, 205-216.

S2. A. Brandner, K. Lehnert, A. Bienholz, M. Lucas and P. Claus, *Topics in Catalysis* 2009, ***52***, 278-287.

S3. D. Liang, C. Shiyu, G. Jing, W. Junhua, C. Ping and H. Zhaoyin, *Chinese Journal of Catalysis* 2011, ***32***, 1831-1837.

S4. X. Ning, Y. Li, H. Yu, F. Peng, H. Wang and Y. Yang, *Journal of Catalysis* 2016, ***335***, 95-104.

S5. S. Feng, J. Yi, H. Miura, N. Nakatani, M. Hada and T. Shishido, *ACS Catalysis* 2020, ***10***, 6071-6083.

S6. M. Zhang, J. Shi, Y. Sun, W. Ning and Z. Hou, *Catalysis Communications* 2015, ***70***, 72-76.

S7. R. Nie, D. Liang, L. Shen, J. Gao, P. Chen and Z. Hou, *Applied Catalysis B: Environmental* 2012, ***127***, 212-220.

S8. W. Hu, D. Knight, B. Lowry and A. Varma, *Industrial & Engineering Chemistry Research* 2010, ***49***, 10876-10882.